Resonant enhanced diffusion in time-dependent flow

P Castiglione†, A Crisanti†, A Mazzino‡§, M Vergassola‡ and A Vulpiani†

† Dipartimento di Fisica, and Istituto Nazionale di Fisica della Materia, Università 'La Sapienza',
P. le A. Moro 2, 00185 Roma, Italy
‡ CNRS, Observatoire de Nice, BP 4229, 06304 Nice Cedex 4, France
§ Dipartimento di Fisica, and Istituto Nazionale di Fisica della Materia, Università di Genova,
Via Dodecaneso 33, 16146 Genova, Italy

Abstract.   Explicit examples of scalar enhanced diffusion due to resonances between different transport mechanisms are presented. Their signature is provided by the sharp and narrow peaks observed in the effective diffusivity coefficients and, in the absence of molecular diffusion, by anomalous transport. For the time-dependent flow considered here, resonances arise between their oscillations in time and either molecular diffusion or a mean flow. The effective diffusivities are calculated using multiscale techniques.

1. Introduction

Passive scalar transport in a given velocity field is an issue of both theoretical and applicative relevance [1, 2]. The combination of molecular and advective effects can lead to rather subtle behaviours, even in the case of simple laminar flow. A rather complete theory has been developed for the dynamics at long times and large scales (macrodynamics), using multiscale techniques [3]. For incompressible velocity fields the macrodynamics in the presence of scale separation is governed by an effective equation which is always diffusive and transport is always enhanced [4]. A sufficient condition ensuring the presence of scale separation for three-dimensional incompressible flow is a vector potential with finite variance, both for static and time-dependent flow [5, 6] (with similar conditions for other space dimensionalities). The small-scale velocity field properties emerge via the effective diffusivity second-order tensor. Its calculation is reduced to the solution of one auxiliary partial differential equation that can be efficiently solved numerically [7, 8] and variational principles have also been derived [9]. The effective diffusivities for generic flow depend on all the mechanisms of transport, e.g. on the advecting velocity field, on the molecular noise, on the presence and the strength of possible mean flow [7, 10]. Each process is characterized by its typical timescales and, if the latter are properly tuned, their mutual interference can produce resonance effects. These lead to strong enhancement of transport, reflected in sharp and narrow peaks in the effective diffusivity. Our aim here is to present explicit examples of such resonance effects in simple time-dependent incompressible velocity fields. In section 2 the source of resonance is the presence of a large-scale velocity field. For random parallel flow (section 2.1), explicit analytic expressions for the effective diffusivities are obtained and they indeed display strong peaks for specific strengths of the large-scale velocity. In section 2.2 the robustness of resonance effects to variations of the scale separation ratio between the large- and the small-scale velocity field components is investigated. Numerical

simulations show that the effects persist even for moderate scale separations. Section 3 is devoted to a time-periodic two-dimensional (2D) flow widely studied to mimic the transport in Rayleigh–Bénard system [11, 12]. The snapshots of the velocity field are made of closed lines. The syncronization between the circulation in the cells and their global oscillation provides, however, for a very efficient way of jumping from cell to cell. This mechanism, similar to stochastic resonance [13, 14], makes the curve of the effective diffusivity versus the frequency ω of oscillation of the flow very structured. In the limit where the molecular diffusion vanishes, anomalous superdiffusion takes place for narrow windows of values of ω around the peaks. The anomaly is observed both in the second-order moment of particle dispersion and in the singular behaviour of the effective diffusivity at high Péclet numbers. In section 4 we study a 2D system consisting of the superposition of steady coherent structures and a random incoherent field with a typical correlation time τ. The resonance occurs now when the sweeping time of the coherent structure is close to τ. Conclusions are reserved for section 5.

2. Parallel flow with a large-scale velocity field

The passive scalar field $\theta(x, t)$ obeys (see [15]) the equation:

$$\partial_t \theta(x, t) + (v \cdot \nabla)\theta(x, t) = D_0 \Delta \theta(x, t). \tag{1}$$

The velocity $v(x, t)$ is assumed here to be incompressible and given by the sum of two terms, u and U. The first is periodic both in space (in a cell of size l) and in time (the technique can be extended with some modifications to handle the case of random, homogeneus and stationary velocity fields). The second is the large-scale component of v, varying on a typical scale L. It is assumed that $l/L = \epsilon \ll 1$, where ϵ is the parameter controlling the scale separation.

We are interested in the dynamics of the field $\theta(x, t)$ on large scales $\sim \mathrm{O}(L)$, comparable to those of U. In the spirit of multiscale methods [3], slow variables $X = \epsilon x$, $T = \epsilon^2 t$ and $\tau_\epsilon = \epsilon t$ are introduced in addition to the fast variables x and t. The time variable τ_ϵ is needed to account for the advective effects generated by the presence of U. The effective equation governing the dynamics at large scales of the field θ is [10]:

$$\partial_t \theta + U \cdot \nabla \theta = \nabla_\alpha D_{\alpha\beta} \nabla_\beta \theta \tag{2}$$

where the second-order eddy-diffusivity tensor is given by

$$D_{\alpha\beta}(X, T) = \delta_{\alpha\beta} D_0 - \tfrac{1}{2}[\langle u_\alpha w_\beta \rangle + \langle u_\beta w_\alpha \rangle] \tag{3}$$

and the symbol $\langle \cdot \rangle$ denotes the average over the periodicities of the small-scale velocity field u. The auxiliary field $w(x, t; X, T)$ has vanishing average over the periodicities and satisfies the equation

$$\partial_t w + [(u + U) \cdot \partial]w - D_0 \partial^2 w = -u. \tag{4}$$

2.1. A solvable case

A well known situation where the effective diffusivities can be calculated analytically is the one of parallel flow. Let us consider in detail the case of three-dimensional random parallel flow in the presence of a large-scale advecting velocity field $U(X, T)$

$$u(x, t) = (u(y, z, t), 0, 0) \qquad U(X, T) = (0, U(X, Z, T), 0). \tag{5}$$

The field $u(x, t)$ is random, homogeneous and stationary. The specific dependence on the spatial variables makes the fields automatically incompressible. The above decomposition

is standard in the framework of mesoscale meteorology [16]. Its physical meaning is that small-scale eddies remain stationary while slow modifications of the large scale component occur. This is quite a common feature in geophysics, e.g. in the planetary boundary layer [17], where the airflow in the thin atmospheric layer near the ground is strongly driven by sink/source forcing terms arising from the bottom boundary.

The first component of the equation (4), the only one for which the r.h.s. does not vanish, can be easily solved in Fourier space and its solution reads

$$\hat{w}_1(\boldsymbol{k}, \omega; \boldsymbol{X}, T) = \frac{-\hat{u}(\boldsymbol{k}, \omega)}{i\omega + k^2 D_0 + i\boldsymbol{U} \cdot \boldsymbol{k}} = -\hat{u}(\boldsymbol{k}, \omega)\hat{G}(\boldsymbol{k}, \omega; \boldsymbol{X}, T) \qquad (6)$$

where the advection-diffusion propagator $\hat{G}(\boldsymbol{k}, \omega; \boldsymbol{X}, T)$ is defined as

$$\hat{G}(\boldsymbol{k}, \omega; \boldsymbol{X}, T) = \frac{1}{i\omega + k^2 D_0 + i\boldsymbol{U} \cdot \boldsymbol{k}} = \int_0^{+\infty} e^{-[i\omega + k^2 D_0 + i\boldsymbol{U} \cdot \boldsymbol{k}]\alpha} \, d\alpha.$$

It follows from (3) that the only non-vanishing elements of the eddy-diffusivity tensor are diagonal and

$$D_{xx}(\boldsymbol{X}, T) = D_0 + \int_0^\infty S(t) \int \hat{E}(\boldsymbol{k}) e^{-[k^2 D_0 + i\boldsymbol{U} \cdot \boldsymbol{k}]t} \, dt \, d\boldsymbol{k} \qquad D_{yy} = D_{zz} = D_0. \qquad (7)$$

We have for simplicity assumed the separability $\hat{E}(\boldsymbol{k}, \omega) = \hat{E}(\boldsymbol{k})\hat{S}(\omega)$, where $\hat{E}(\boldsymbol{k})$ and $\hat{S}(\omega)$ are the spectra of the spatial and the temporal part of the correlation function of $\boldsymbol{u}$.

The simple analytic expression (7) can be used to address the question of interest in this paper, i.e. whether it is possible to have a resonance between the oscillation frequencies induced by U and the small-scale velocity field. We shall assume for simplicity U to be independent of both $\boldsymbol{X}$ and T, the wavenumber $\boldsymbol{k}$ along the direction of $\boldsymbol{U}$ (so that $\boldsymbol{k} \mapsto k$), and the following temporal part of the velocity correlation function

$$S(t) = e^{-|t|/\tau} \cos(\omega t). \qquad (8)$$

Substituting (8) into (7) and performing a simple integration, the latter (omitting the subscript 'xx') takes the form

$$D = D_0 + \tau_0 \int_0^\infty \hat{E}(k) R(k) \, dk. \qquad (9)$$

Here, the function $R(k)$ is

$$R(k) = \frac{\left(\frac{1+\omega^2\tau^2}{1+k^2 D_0\tau}\right)\left[1 + \left(\frac{\omega\tau}{1+k^2 D_0\tau}\right)^2 + \left(\frac{U\tau k}{1+k^2 D_0\tau}\right)^2\right]}{\left[1 + \left(\frac{\omega\tau}{1+k^2 D_0\tau}\right)^2 + \left(\frac{Uk\tau}{1+D_0 k^2\tau}\right)^2\right]^2 - 4\left[\frac{\omega U k\tau^2}{(1+D_0 k^2\tau)^2}\right]^2} \qquad (10)$$

and τ_0 is the correlation time of turbulence

$$\tau_0 = \int_0^\infty S(t) \, dt = \frac{\tau}{1 + \omega^2\tau^2}. \qquad (11)$$

Note that $R(k) \to 1$ when both $U \to 0$ and $D_0 \to 0$. In the latter case $D = u_0^2\tau_0$ ($u_0^2 = \int dk\, E(k)$), the well known result valid for velocity fields δ-correlated in time (see, e.g. [8]). It follows from (9) that the combined effect of D_0 and U is to modify the correlation time of turbulence, producing an effective correlation time $\tau_{\text{eff}} = \tau_0 R(k)$, which depends on the wavenumber k. It is precisely such a dependence on k that makes it possible

to have resonances. Let us indeed consider (10) for a vanishing value of D_0. It is easy to verify that, for $\omega\tau > 1/\sqrt{3}$, $R(k)$ has a peak for

$$U^{\text{res}} = \frac{1}{k\tau}\sqrt{-\omega^2\tau^2 - 1 + 2\omega\tau\sqrt{\omega^2\tau^2 + 1}}.$$ (12)

In the limit $\omega\tau \gg 1$, the previous expression reduces to: $U^{\text{res}} = \omega/k$. Note that $R(k)$ crosses the unit value for $\omega\tau > 1/\sqrt{3}$. The regime $R(k) > 1$ corresponds to constructive interference between the turbulent motion and the slow-varying one [18]. In contrast, destructive interference takes place, for $\omega\tau \leqslant 1/\sqrt{3}$ where $R(k)$ monotonically decreases from 1 ($U = 0$) to zero (large U). The effective diffusivity for small-scale flows with a single wavenumber k_0, attains at the maximum the value

$$D^{\text{res}} = u_0^2\tau_0\frac{(1 + \omega^2\tau^2)(1 + 2\omega^2\tau^2)}{1 + 4\omega^2\tau^2}.$$ (13)

When $\omega\tau \gg 1$ (and the velocity U is 'synchronized' with the oscillating velocity field ($U^{\text{res}} = \omega/k_0$)), the previous expression reduces to $u_0^2\tau_0\frac{\omega^2\tau^2}{2}$. For $U \gg \omega/k_0$, the effective diffusivity D goes to zero quadratically, as $D = u_0^2\tau_0(\frac{\omega}{k_0 U})^2$.

The final result is that for a random parallel flow periodic in a box of size L ($k_0 = 2\pi/L$) and $\omega\tau \gg 1$, the peaks of the effective diffusivity D occur for

$$U_n^{\text{res}} = \frac{\omega}{k_0 n} \qquad n = 1, 2, \ldots,$$ (14)

with values given, for large U, by

$$D_n^{\text{res}} \sim \hat{E}(k_0 n)\tau_0\frac{\omega^2\tau^2}{2}.$$ (15)

The behaviour of D as a function of U, obtained evaluating numerically the integral (9), is shown in figure 1 for a Kolmogorov spectrum $\hat{E}(k) \propto k^{-5/3}$, and for three different values of $\omega\tau \geqslant 1/\sqrt{3}$. Peaks of enhanced diffusion are evident for values of U given by (14). Note that for $\omega\tau = 40$, the first five peaks of D (from right to left) are close to the values given by the expression (15).

The role of a non-vanishing molecular diffusivity D_0 is to reduce the height of the peaks. This point is shown in figure 2, where the behaviour of $D/(u_0^2\tau_0)$ is plotted as a function of $Uk_0\tau$, for $\omega\tau = 40$ and for three different values of D_0. As we shall see in the following, these features hold also for more general flows than those considered in this section.

It is finally worth noting that parallel flow permits us to present yet another simple example of resonance. Considering indeed the expression (9) for vanishing values of U, it is easy to verify that for

$$D_0 = \frac{\omega\tau - 1}{k^2\tau} \sim \frac{\omega}{k^2}$$ (16)

peaks of D occur. This corresponds to a synchronization between the characteristic viscous frequency $k^2 D_0$ of the random molecular noise and the frequency ω of the oscillatory velocity field.

2.2. Parallel flow with moderate scale separations

The aim here is to show that the resonant enhanced diffusion previously discussed also appears when only moderate scale separation factors are present. As in (1), consider indeed the velocity field $v = u + U$ with u parallel to the x-axis
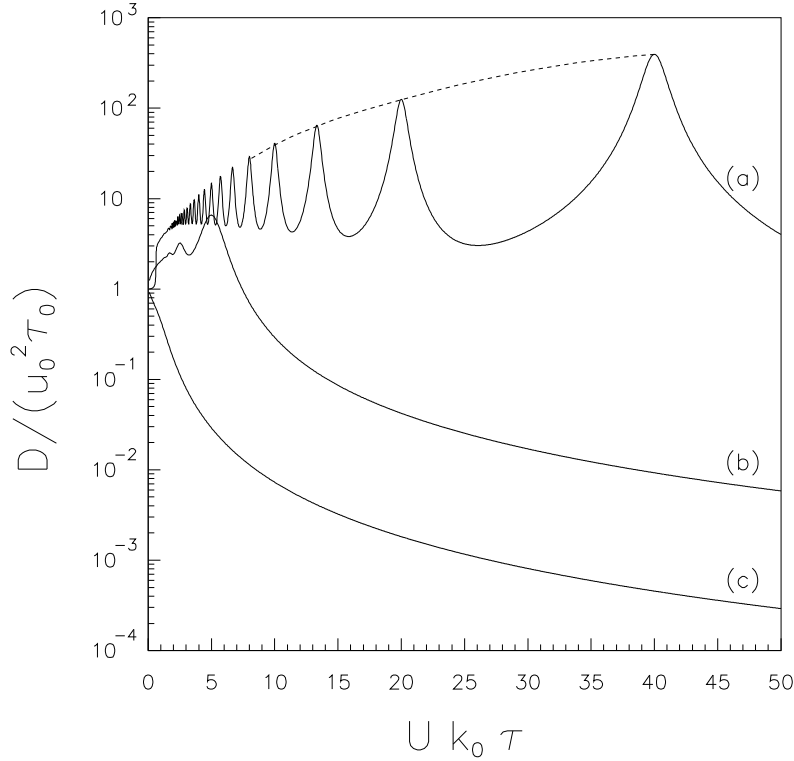
$$u = (u_1\cos(k_1 y + \omega_1 t), 0, 0)$$ (17)

Figure 1. The eddy-diffusivity $D/(u_0^2\tau_0)$ versus the mean flow strength $Uk_0\tau$. The curve is obtained by numerical integration of (9) for $D_0 = 0$, $\hat{E}(k) \propto k^{-5/3}$, temporal correlation function $S(t) = e^{-|t|/\tau}\cos(\omega t)$ and Strouhal number $S \equiv u_0\tau_0 k_0 \sim 1$. The three curves correspond to (a): $\omega\tau = 40$; (b): $\omega\tau = 5$; (c): $\omega\tau = 1/\sqrt{3}$. The broken curve joins the peaks of D given by the expression (15) for $n = 1, 2, \ldots, 5$.

and U parallel to the y-axis

$$U = (0, u_2\cos(k_2 x + \omega_2 t), 0) \tag{18}$$

and $k_1 > k_2$. The situation $k_1 \gg k_2$ corresponds to the scale-separated case previously considered. Here, we shall assume $k_1 = 2.5k_2$ (and $u_1 = u_2$) and we shall be interested in the dynamics at scales much larger than $1/k_2$. The two components of the velocity field v have moderate scale separation and affect transport on equal footing. The velocity v not being a parallel flow, analytical expressions for the effective diffusivities D_{ij} are no longer available. We had then to solve numerically the standard auxiliary equation arising from multiscale methods (see, e.g. [8]). The equation is solved by using a pseudo-spectral method [21] in the basic periodicity cell with a grid mesh of 64×64 points. De-aliasing has been obtained by a proper circular truncation which ensures better isotropy of numerical treatment. Time marching has been performed using a leap-frog scheme mixed with a predictor–corrector scheme (see [22]) at regular intervals.

To enlighten the resonant diffusion enhancement, ω_1 is fixed and the D_{ij} behaviour as a function of ω_2 is investigated. Results are reported in figures 3 and 4, where $D_{ii}/(u_0^2\tau_1)$ versus $4\omega_2/\omega_1$ is presented for different values of D_0. Here, $u_0^2 = u_1^2 + u_2^2$ and $\tau_1 = 2\pi/\omega_1$ is the oscillation period of the small-scale component. Results clearly exhibit resonance peaks for $\omega_2 = \omega_1$, $\omega_2 = \omega_1/2$, $\omega_2 \sim \omega_{sw}$ and $\omega_2 \sim 2\omega_{sw}$, where the frequency ω_{sw} is
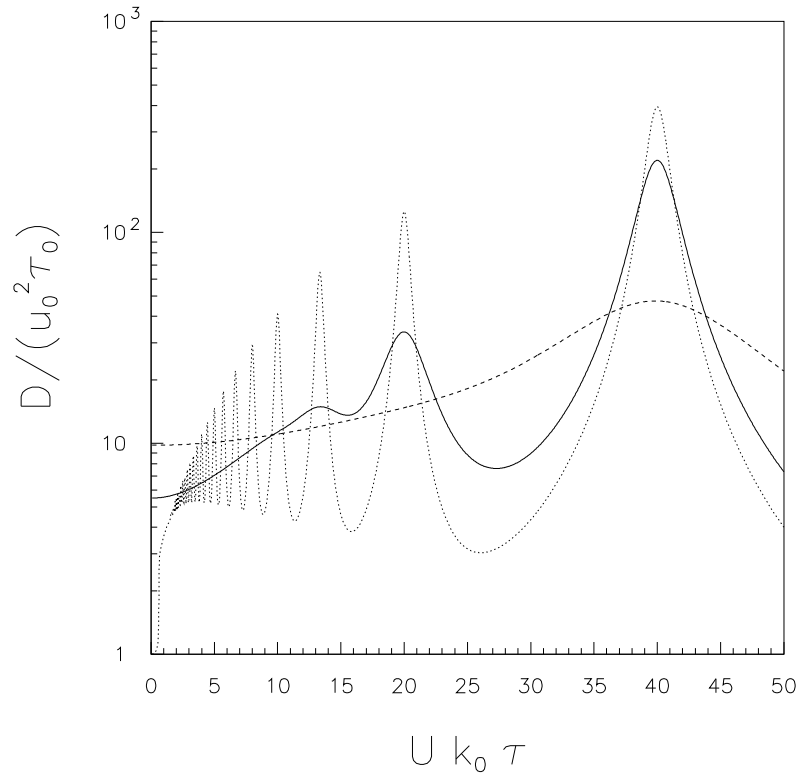
Figure 2. The same as in figure 1, but the behaviour of $D/(u_0^2\tau_0)$ is now plotted for three different values of D_0 and $\omega\tau = 40$. Dotted curve: $D_0 = 0$; full curve: $D_0/(u_0^2\tau_0) = 5 \times 10^{-4}$; broken curve: $D_0/(u_0^2\tau_0) = 5 \times 10^{-3}$. Note that the larger D_0 is, the broader are the peaks.

defined as

$$\omega_{sw} = \frac{2\pi}{T_{sw}} \qquad \text{with } T_{sw} = \frac{L}{u_0}$$

and $4\omega_{sw}/\omega_1 = \sqrt{2}$. There are other peaks for $\omega < \omega_{sw}$, corresponding to submultiples of ω_1 and ω_{sw}.

Note in figure 4 that D_{22} increases for $\omega_2 \rightarrow 0$. This is qualitatively understood as follows. For small ω_2, the velocity field is essentially a stationary shear flow in the y-direction superimposed to a rapidly changing small-scale component. The picture is rather close to the Taylor mechanism for the longitudinal diffusion in the shear flow, which is known to lead to a $1/D_0$ behaviour for D_{22} [23].

3. Diffusion in time-periodic Rayleigh–Bénard convection

Let us consider the two-dimensional velocity field defined by the following stream function

$$\psi(x, y, t) = \psi_0 \sin(x + B \sin \omega t) \sin y. \tag{19}$$

This flow [11, 12] is a simple model for transport in time-periodic Rayleigh–Bénard convection. The stream function (19) describes a single-mode, two-dimensional convection with a rigid boundary condition. The even oscillatory instability [19] is accounted for by
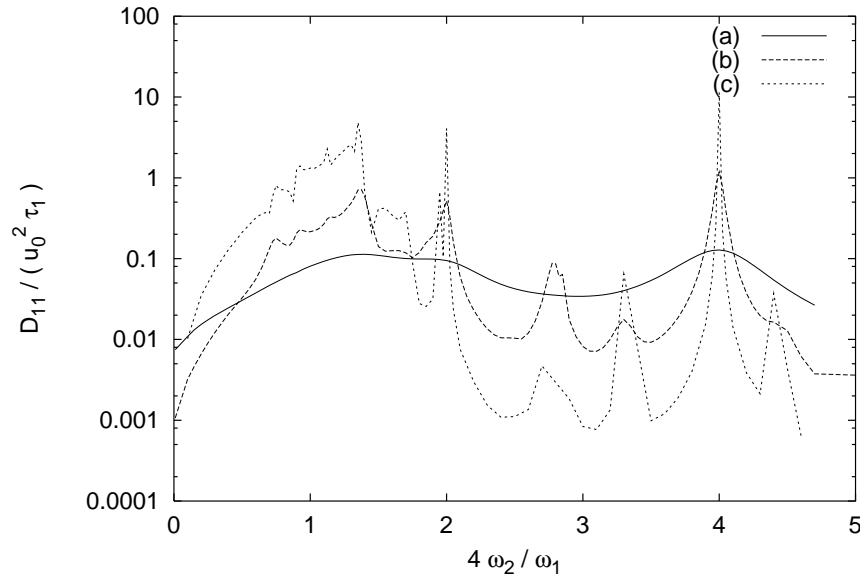
Figure 3. The non-dimensional eddy-diffusivity $D_{11}/(u_0^2\tau_1)$ versus the non-dimensional frequency $4\omega_2/\omega_1$, for different values of $D_0/(u_0^2\tau_1)$. The cases (a), (b) and (c) correspond to $D_0/(u_0^2\tau_1) = 3 \times 10^{-3}$, $D_0/(u_0^2\tau_1) = 3 \times 10^{-4}$ and $D_0/(u_0^2\tau_1) = 3 \times 10^{-5}$, respectively.
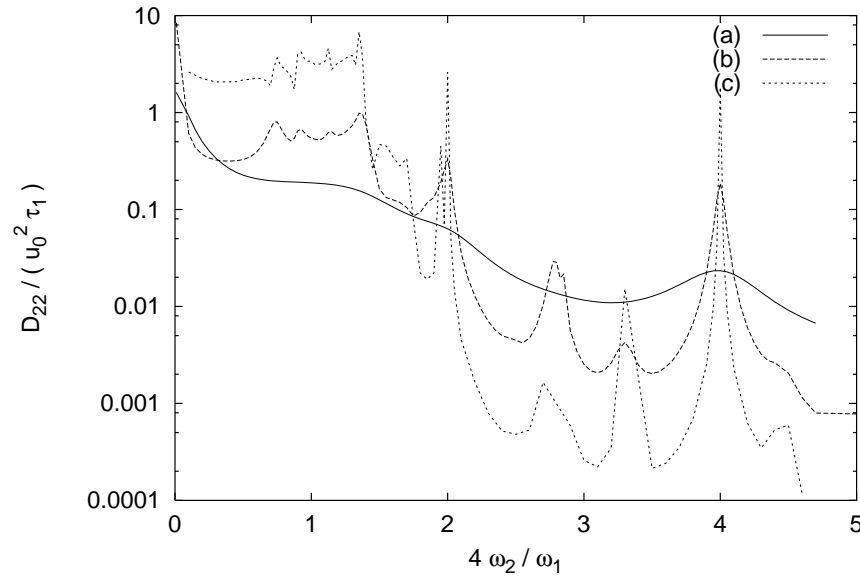

Figure 4. The non-dimensional eddy-diffusivity $D_{22}/(u_0^2\tau_1)$ versus the non-dimensional frequency $4\omega_2/\omega_1$, for different values of $D_0/(u_0^2\tau_1)$. The cases (a), (b) and (c) correspond to $D_0/(u_0^2\tau_1) = 3 \times 10^{-3}$, $D_0/(u_0^2\tau_1) = 3 \times 10^{-4}$ and $D_0/(u_0^2\tau_1) = 3 \times 10^{-5}$, respectively.

the term $B\sin\omega t$, representing the lateral oscillation of the roll. In [12], a quantitative comparison of the behaviour in this flow with the experimental data has shown that the basic mechanisms of convective transport are well captured by the expression (19).

For a fixed ωt, the oscillation frequency of a Lagrangian particle close to the centre of the periodic cell is of the order of ψ_0. The periodicity of the cell is $L \equiv 2\pi$ and the dimensionless parameter controlling the dynamics is $\epsilon = \omega L^2/\psi_0$. The two limiting regimes $\epsilon \ll 1$ and $\epsilon \gg 1$ have been investigated in [20] to obtain the expressions of the diffusion coefficients in the limit of zero molecular diffusivity. Here, we shall concentrate on the behaviour for $\epsilon \sim 1$. It is indeed precisely in this region that a synchronization between the characteristic frequencies $O(\psi_0)$ and $O(\omega)$ can take place. In all the cases reported here, a resolution 512×512 has been used, which is found adequate for molecular diffusivities $D_0/\psi_0 \geqslant 5 \times 10^{-4}$. The system evolution has been computed up to times $500L^2/\psi_0$, with a time step $\Delta t = 10^{-2}L^2/\psi_0$.

For small enough (or vanishing) molecular diffusivities, the numerical integration of the partial differential equation (4) is clearly subject to instabilities. To evaluate the eddy-diffusivities, it is then more convenient to integrate the equation $d_t \boldsymbol{x} = \boldsymbol{v}$ for the coordinates $\boldsymbol{x}(t)$'s of the Lagrangian particles. This is made by using a second-order Runge–Kutta scheme and then performing a linear fit of $\langle [x(t) - x(0)]^2 \rangle$ versus t, to obtain the diffusion coefficient. The averages are made over different realizations and are performed by uniformly distributing 10^6 particles in the basic periodic cell. The system evolution has been computed up to times $10^4 L^2/\psi_0$. Numerical schemes have been tested both for vanishing values of ω and for large Péclet number. Asymptotic solutions for the effective diffusivity are indeed available in these limits (see equation (27) in [24]). Measured diffusion coefficients agree with the theoretical values within errors of less than 1%.

The turbulent diffusivity (the x-component) versus the frequency $\omega L^2/\psi_0$ is shown in figure 5 for different values of D_0/ψ_0. A few comments are in order. First, the turbulent diffusivity shows maxima which seem similar to those observed for stochastic resonance [13, 14]. Here, the resonance is between the lateral roll oscillation frequency and the characteristic frequencies of the scalar field motion. Second, the effect of D_0 on the shape of the peaks is twofold: similarly to the case of the parallel flow, the smaller is D_0, the sharper are the peaks. Furthermore, from the expanded view of figure 5(*a*), it appears that variations of D_0 also cause a shifting of maxima positions.

For $D_0 \rightarrow 0$, the peak shown in figure 5 moves toward $\omega L^2/\psi_0 \sim 1.1$ and the transport becomes superdiffusive at $D_0 = 0$, i.e. the mean-squared displacement is superlinear:

$$\langle [x(t) - x(0)]^2 \rangle \propto t^\alpha \qquad \text{with } \alpha > 1. \tag{20}$$

The range of $\omega L^2/\psi_0$ values where the process is superdiffusive turns out to be very narrow: for $\omega L^2/\psi_0 = 1.1$ the mean-squared displacement behaviour is given by (20) with exponent $\alpha \sim 1.3$; both for $\omega L^2/\psi_0 = 1.075$ and $\omega L^2/\psi_0 = 1.15$ the diffusion process is standard (i.e. $\alpha = 1$). This point is illustrated in figure 6, where the mean-squared displacement as a function of the time is shown in a log–log plot for $\omega L^2/\psi_0 = 1.075$, $\omega L^2/\psi_0 = 1.1$ and $\omega L^2/\psi_0 = 1.15$.

A more careful test of the anomalous diffusion at $D_0 = 0$ consists in computing the diffusion coefficient D as function of D_0. As suggested in [8], in the presence of genuine anomalous diffusion, the effective diffusivity must diverge and it is expected that $D \sim D_0^{-\beta}$ with $\beta > 0$. The curve D versus D_0 at $\omega L^2/\psi_0 = 1.1$ is shown in figure 7. The data are well fitted by a straight line with slope $\beta \sim 0.18$, confirming the presence of anomalous diffusion at $D_0 = 0$.
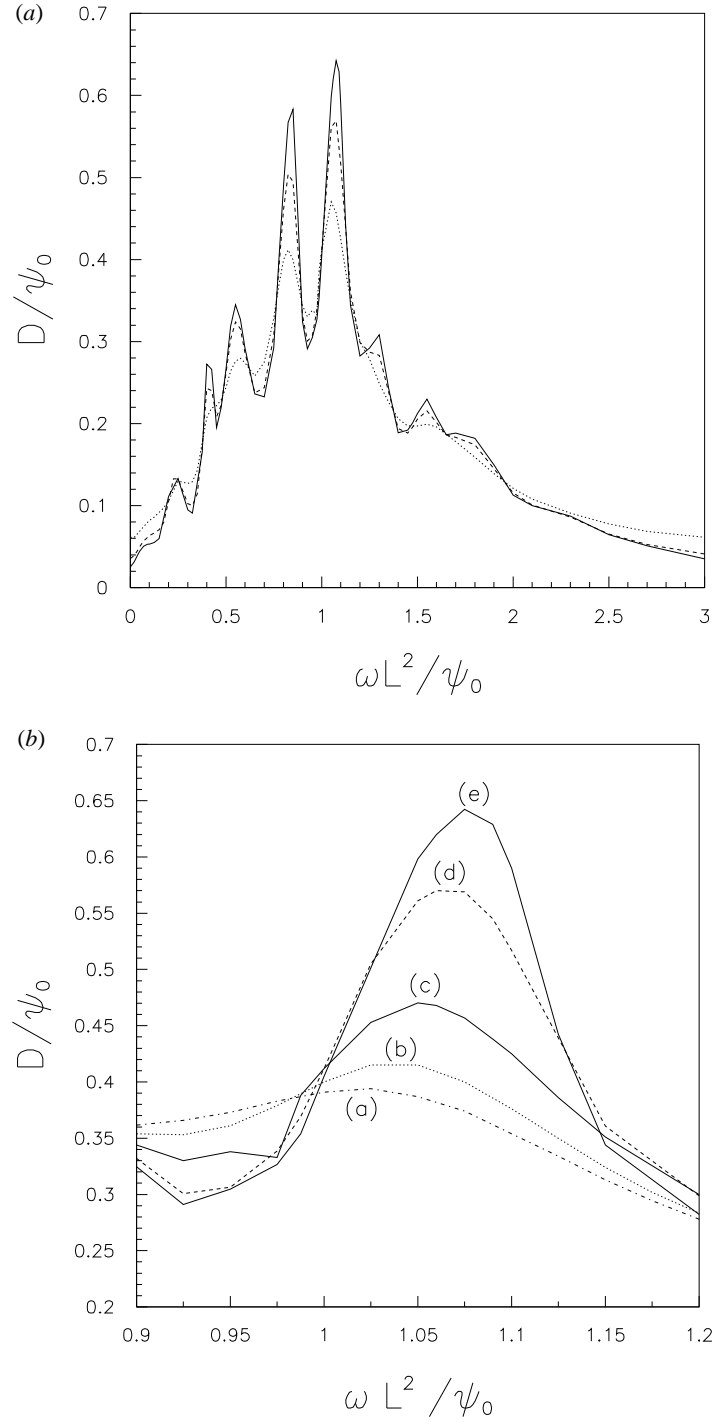
Figure 5. The turbulent diffusivity D/ψ_0 versus the frequency $\omega L^2/\psi_0$ for different values of the molecular diffusivity D_0/ψ_0. (*a*): $D_0/\psi_0 = 3 \times 10^{-3}$ (dotted curve); $D_0/\psi_0 = 1 \times 10^{-3}$ (broken curve); $D_0/\psi_0 = 5 \times 10^{-4}$ (full curve). (*b*): $D_0/\psi_0 = 1 \times 10^{-2}$ (a); $D_0/\psi_0 = 6 \times 10^{-3}$ (b); $D_0/\psi_0 = 3 \times 10^{-3}$ (c); $D_0/\psi_0 = 1 \times 10^{-3}$ (d); $D_0/\psi_0 = 5 \times 10^{-4}$ (e).
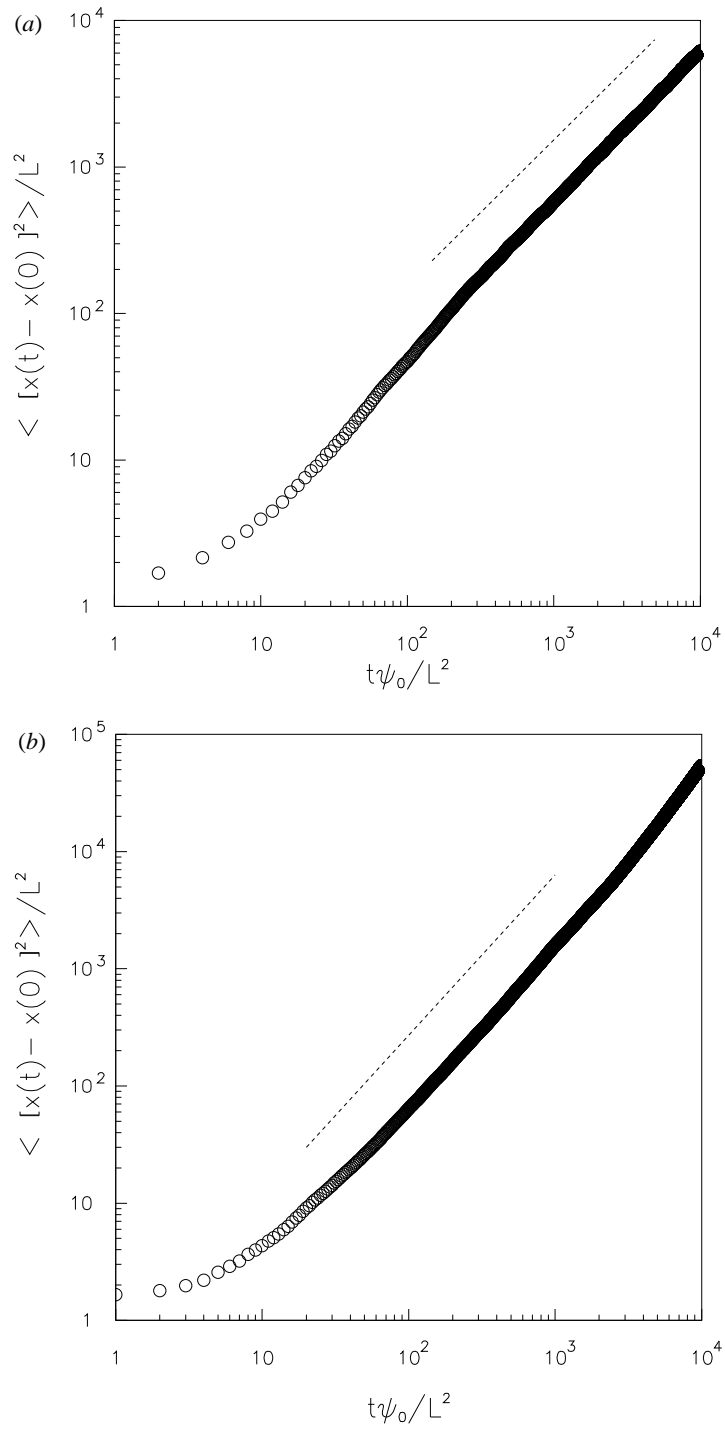
(*a*)

(*b*)

Figure 6. The mean-squared displacement versus the time for the flow (19) with $D_0 = 0$ (in a log–log scale). (*a*): $\omega L^2/\psi_0 = 1.075$, (*b*): $\omega L^2/\psi_0 = 1.1$ and (*c*): $\omega L^2/\psi_0 = 1.15$. Broken lines have slopes 1, 1.3 and 1, respectively.
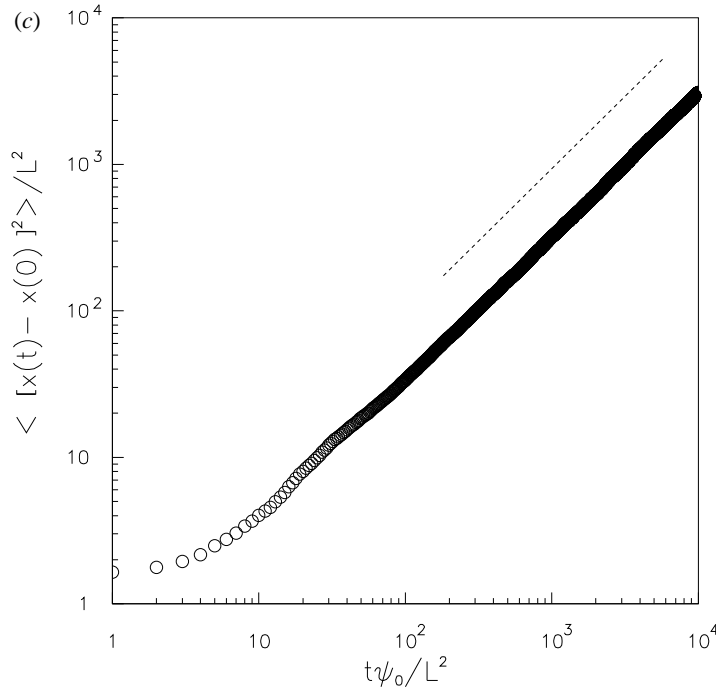
Figure 6. (Continued.)

4. Enhanced diffusion in the presence of coherent structures

We shall consider now the case where the two-dimensional large-scale component U consists of a coherent structure. The small-scale part u is random. Specifically, $u = (u_1, u_2)$, where the u_i's are homogeneous, isotropic and stationary Gaussian random processes. Their Fourier transforms $\hat{u}_i$ have zero mean and correlation functions

$$\langle \hat{u}_i(\boldsymbol{k}, t)\hat{u}_j(\boldsymbol{k}', t')\rangle = (2\pi)^2 \delta(\boldsymbol{k} + \boldsymbol{k}')\hat{R}_{ij}(\boldsymbol{k})T(\boldsymbol{k}, t - t') \tag{21}$$

where

$$\hat{R}_{ij}(\boldsymbol{k}) = (\delta_{ij}k^2 - k_i k_j)f(k) \qquad \text{and} \qquad T(\boldsymbol{k}, t - t') = \mathrm{e}^{-\frac{|t-t'|}{\tau(k)}}.$$

The $f(k)$ function is related to the field energy spectrum $E(k)$ as follows:

$$E(k) = \frac{1}{2\pi}k^3 f(k).$$

The following expressions for $E(k)$ and $\tau(k)$ have been considered

$$E(k) = \begin{cases} Ak^3 & k \in [0, k_m^I] \\ Bk^{-\frac{5}{3}} & k \in [k_m^I, k_M^I] \\ Ce^{-k} & k > k_M^I \end{cases} \tag{22}$$

and

$$\tau(k) = \begin{cases} Dk^{-3} & k \in [0, k_m^I] \\ Fk^{-\frac{2}{3}} & k \in [k_m^I, k_M^I] \\ Gk^{-\frac{3}{2}}\mathrm{e}^{\frac{k}{2}} & k > k_M^I \end{cases} \tag{23}$$
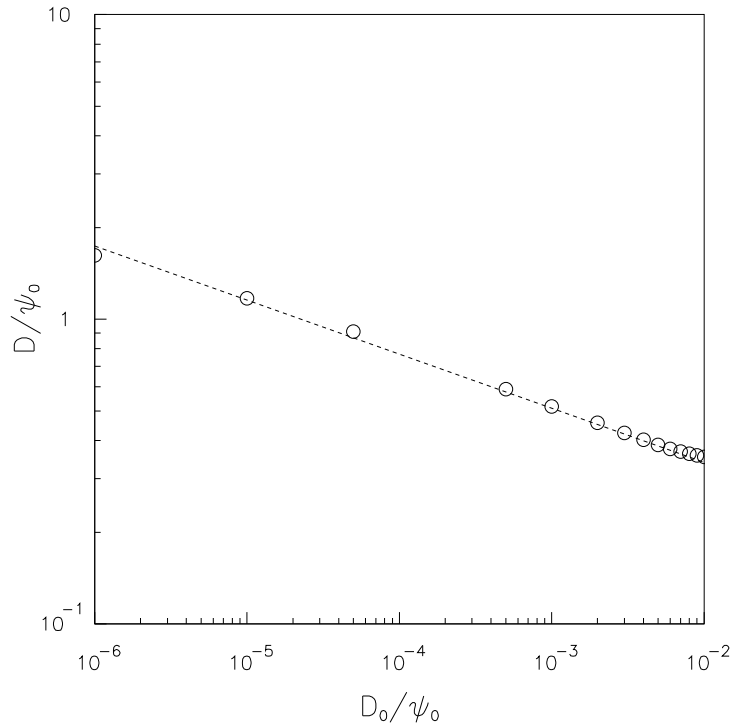
Figure 7. The diffusion coefficient D as a function of D_0 at $\omega L^2/\psi_0 = 1.1$ (in a log–log scale). The slope of the broken line is $-\beta \sim 0.18$.

where the constants A, C and D, G are chosen to ensure the continuity of $E(k)$ and $\tau(k)$ in k_m^I and k_M^I, respectively. The expression for $\tau(k)$ is meant to mimic 3D turbulence, neglecting intermittency and correlations between phases. The $\hat{u}_i(\boldsymbol{k}, t)$ can be easily generated by a linear Langevin equation. The coherent large-scale component has the cellular structure

$$U = U(\cos y, \cos x) \tag{24}$$

characterized by the typical Lagrangian time $T_c = \pi/(\sqrt{2}U)$. From the isotropy of the field it follows that $D_{11} = D_{22} \equiv D$. In figure 8 the diffusion coefficient $D/(u_0^2\tau_1)$ is shown as a function of T_c/τ_1, where $\tau_1 = \tau(k_m^I)$ is a characteristic timescale of the random field and $u_0^2 = \int dk\, E(k)$.

   The above results have been obtained performing direct numerical simulations of the auxiliary equation (4) (now $U = 0$ and $\boldsymbol{u}$ has the spectrum defined by (22)) by using a pseudo-spectral method over the periodic box $2\pi \times 2\pi$ with a resolution 64×64.

   It is well evident that the presence of a peak for $T_c/\tau_1 \sim 7$ and $D_0/(u_0^2\tau_1) = 3.9 \times 10^{-4}$, whose value is $D/(u_0^2\tau_1) \sim 0.86$. The fact that the peak does not appear for T_c/τ_1 of the order of unity is most likely due just to the freedom in the definition of the characteristic times T_c and τ_1. In contrast, it is important to note that the value of the peak is much larger than the one occurring when either the random field or the coherent structure are absent. The value $D/(u_0^2\tau_1) \sim 0.86$ has in fact to be compared with 0.07 and 0.32, respectively.

   Unlike the resonance in the Reyleigh–Bénard convection, the syncronization mechanism produces here a broad peak. This is not surprising as in this case the random field has a wide spectrum of characteristic times.
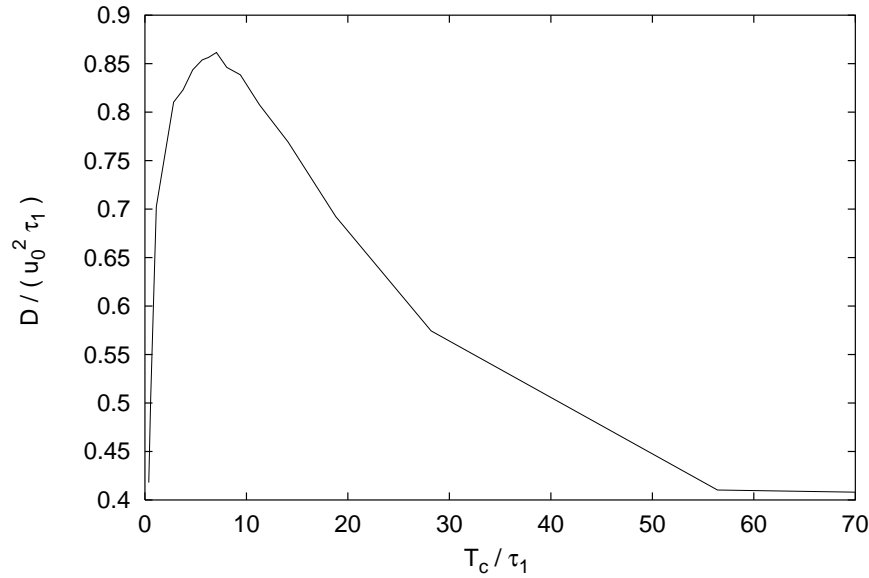
Figure 8. The non-dimensional eddy-diffusivity $D/(u_0^2\tau_1)$ versus the non-dimensional Lagrangian time T_c/τ_1 for $D_0/(u_0^2\tau_1) = 3.9 \times 10^{-4}$ and $k_M^I/k_m^I = 4.5$.

5. Conclusions

Multiscale techniques have been used to present a series of explicit examples of strong diffusion enhancement due to resonance effects between different transport mechanisms. The effects appear already from the analytical expression of eddy-diffusivity for random flows with a large-scale mean flow component, are robust to a reduction of the scale separation and they are also observed in convective transport and when coherent structures are present on the large scales. For vanishing molecular diffusivities and for specific values of the control parameters, the enhanced diffusion might turn into anomalous superdiffusion. Finally, let us stress in which respect the resonant enhanced diffusion effects discussed in this paper differ from other known mechanisms to produce strong transport. For Taylor longitudinal diffusion in shear flow, open streamlines producing large effective diffusivities are, for example, present in the snapshots of the velocity field itself. For the convective flow in section 3, snapshots of the velocity field are always made of closed streamlines. Open streamlines, and more generally enhanced transport, have a dynamical origin and require a temporal syncronization between different transport mechanisms.

Acknowledgments

References

[1]   Moffatt H K 1983 *Rep. Prog. Phys.* **46** 621
[2]   Crisanti A, Falcioni M, Paladin G and Vulpiani A 1991 *Riv. Nuovo Cimento* **14** 1
[3]   Bensoussan A, Lions J-L and Papanicolaou G 1978 *Asymptotic Analysis for Periodic Structures* (Amsterdam: North-Holland)
[4]   McLaughlin D, Papanicolaou G C and Pironneau O 1985 *SIAM J. Appl. Math.* **45** 780
[5]   Avellaneda M and Majda A 1991 *Commun. Math. Phys.* **138** 339
[6]   Avellaneda M and Vergassola M 1995 *Phys. Rev.* E **52** 3249
[7]   Majda A and McLaughlin R 1993 *Stud. Appl. Math.* **89** 245
[8]   Biferale L, Crisanti A, Vergassola M and Vulpiani A 1995 *Phys. Fluids* **7** 2725
[9]   Fannjang A and Papanicolau G C 1994 *SIAM J. Appl. Math.* **54** 333
[10] Mazzino A 1997 *Phys. Rev.* E **56** 5500
[11] Gollub J P and Solomon T H 1988 *Proc. Fritz Haber Int. Symp.* ed I Procaccia (New York: Plenum)
[12] Solomon T H and Gollub J P 1988 *Phys. Rev.* A **38** 6280
[13] Benzi R, Sutera A and Vulpiani A 1981 *J. Phys.* **14** L453
[14] Benzi R, Parisi G, Sutera A and Vulpiani A 1983 *SIAM J. Appl. Math.* **43** 565
[15] Chandrasekhar S 1943 *Rev. Mod. Phys.* **15** 1
[16] Pielke R 1984 *Mesoscale Meteorological Modeling* (Orlando, FL: Academic)
[17] Sorbjan Z 1989 *Structure of the Atmospheric Boundary Layer* (Englewood Cliffs, NJ: Prentice-Hall)
[18] Mazzino A and Vergassola M 1997 *Europhys. Lett.* **37** 535
[19] Clever R M and Busse F H 1974 *J. Fluid Mech.* **65** 625
[20] Chernikov A A, Neishtadt A I, Rogal'sky A V and Yakhnin V Z *Chaos* **1** 206
[21] Gottlieb D and Orszag S A 1977 *Numerical Analysis of Spectral Methods* (Philadelphia, PA: SIAM)
[22] Marchuk G I 1975 *Methods of Numerical Mathematics* (New York: Springer)
[23] Taylor G I 1953 *Proc. R. Soc.* A **219** 186
      Taylor G I 1954 *Proc. R. Soc.* A **225** 473
[24] Rosembluth M N, Berk H L, Doxas I and Horton W 1987 *Phys. Fluids* **30** 2636